

## Getz Ice Shelf melting response to changes in ocean forcing

S. Jacobs,<sup>1</sup> C. Giulivi,<sup>1</sup> P. Dutrieux,<sup>2</sup> E. Rignot,<sup>3,4</sup> F. Nitsche,<sup>1</sup> and J. Mouginot<sup>3,4</sup>

Received 12 March 2013; revised 14 June 2013; accepted 29 June 2013; published 5 September 2013.

[1] The large and complex Getz Ice Shelf extends along nearly half of the West Antarctic coastline in the Amundsen Sea and is exposed to a more variable ocean environment than most other Pacific sector ice shelves. Ocean temperature, salinity, and dissolved oxygen profiles acquired near its sub-ice cavity openings are used here to estimate seawater transports and meltwater fractions. More complete coverage during 2000 and 2007 brackets most of the variability observed from 1994 to 2011, and yearlong records near one ice front support the use of summer profiles to determine annual basal melt rates. We find area average rates of 1.1 and 4.1 m/yr, higher in 2007 when a larger volume of warmer deep water occupied the adjacent continental shelf, and the ocean circulation was stronger. Results are consistent with changes in thermocline depths relative to ice shelf draft and mass transports onto the adjacent continental shelf. We also calculate steady state and actual melting of 2.5 and 4.6 m/yr in 2007–2008 from satellite measurements of ice flux, modeled accumulation, and thinning from 2003 to 2008. This implies a positive mass balance in 2000, but negative in 2007, when the Getz was producing more meltwater than any of the larger, slower melting or smaller, faster-melting ice shelves.

**Citation:** Jacobs, S., C. Giulivi, P. Dutrieux, E. Rignot, F. Nitsche, and J. Mouginot (2013), Getz Ice Shelf melting response to changes in ocean forcing, *J. Geophys. Res. Oceans*, 118, 4152–4168, doi:10.1002/jgrc.20298.

### 1. Background

[2] Discovered during the 1939–1941 US Antarctic Service Expedition and initially charted from air photos in 1946–1947 and 1962–1965 [Alberts, 1995], the Getz Ice Shelf (GIS) spans ~650 km of the Pacific–Antarctic coastline between 115° and 135°W in the central and western Amundsen Sea (Figure 1). An area of 33,395 km<sup>2</sup> from Rignot *et al.* [2013]—minus small shelfy areas on the north sides of Carney and Siple Islands—exceeds that of other ice shelves in the SE Pacific sector and is slightly larger than the 1997 area including ice rises in Swinbank *et al.* [2003a, 2003b]. While the Getz lacks a large ice sheet drainage basin and is not dominated by inflow from a single, fast-moving glacier, satellite observations have shown declining elevations of grounded ice along its southern perimeter [Rignot *et al.*, 2008; Pritchard *et al.*, 2009; Zwally and Giovinetto, 2011]. Islands that anchor the northern ice shelf perimeter will constrain iceberg calving, and internal

grounded regions [Swinbank *et al.*, 2003a, 2003b; Rignot *et al.*, 2011a] may influence the sub-ice ocean cavity circulation. East-west differences in elevation change [Zwally *et al.*, 2005; Pritchard *et al.*, 2012] could also reflect spatial variability in ocean forcing. Decreasing surface elevations combined with firm modeling have revealed ice shelf thinning, inferred to result from basal melting [Pritchard *et al.*, 2012]. Actual melt rates could be more or less than needed to account for thinning or ice shelf mass balance.

[3] Circumpolar Deep Water (CDW) extends beneath deep-draft ice shelves in the eastern Amundsen Sea, causing strong basal melting, thinning, and accelerated glacier flow into Pine Island Bay (PIB) [Jacobs *et al.*, 1996, 2011; Shepherd *et al.*, 2004; Rignot, 2008; Jenkins *et al.*, 2010]. Near the GIS, deep water on the continental shelf is cooler and fresher, more closely resembling the CDW in PIB than the highly modified deep water (MCDW) near the Ross Ice Shelf [Jacobs and Giulivi, 2010; Jacobs *et al.*, 2012] and will be referred to here as mCDW. Spatially variable oceanic forcing might be expected under the Getz because of its length, multiple openings to the sea, and location between the warmer Bellingshausen and colder Ross Sea regimes. To the east, CDW warmer than 1°C is overlain in summer by surface water freshened by melting and high precipitation (Figure 2). To the west, MCDW and surface waters are converted by strong sea ice production and export into salty, near-freezing shelf waters. The GIS also lies south of possible intermittent eastward extensions and accelerations of the Ross Gyre [Assmann and Timmermann, 2005a; Holland and Kwok, 2012], likely to influence ocean

<sup>1</sup>Lamont-Doherty Earth Observatory, Columbia University, Palisades, New York, USA.

<sup>2</sup>British Antarctic Survey, NERC, Cambridge, UK.

<sup>3</sup>Jet Propulsion Laboratory, Pasadena, California, USA.

<sup>4</sup>Department of Earth System Science, University of California, Irvine, California, USA.

Corresponding author: S. S. Jacobs, Lamont-Doherty Earth Observatory, 205 Oceanography, Route 9W, Palisades, NY 10964, USA. (sjacobs@ldeo.columbia.edu)

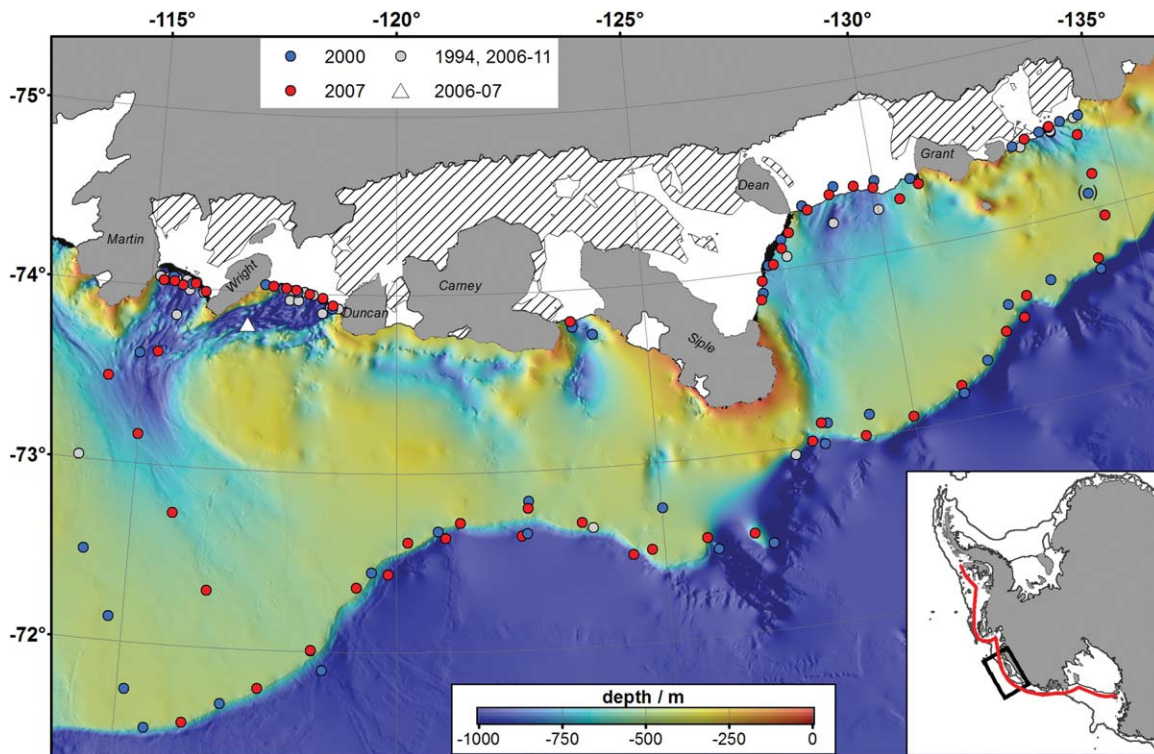


**Figure 1.** Getz Ice Shelf (GIS) occupies the southern quarter of the western and central Amundsen Sea continental shelf [Nitsche *et al.*, 2007] and  $\sim 20^\circ$  of longitude along the Pacific coastline of the West Antarctic Ice Sheet (inset, with the red line locating Figures 2 and 3). The GIS area is striped where Bedmap2 ice drafts [Fretwell *et al.*, 2013] exceed a mean of  $\sim 400$  m (Figure 4). Colored/gray circles position CTD profiles (one shifted) used in Figures 2–9 and 11. The triangle near Wright Island identifies the site of 2006–2007 time series records in Figure 6. Rougher seafloor bathymetry on the inner continental shelf defines glacially scoured troughs that deepen toward ice fronts between the pinning islands.

properties and circulation on the adjacent continental shelf. Temporal variability is also evident along the southeast Pacific-Antarctic coastline, with deep waters warmer and upper water column salinities lower in 2007 than in 1994 in the Amundsen sector (Figure 3). That salinity decline deepens westward and becomes incorporated into shelf water formation in the freshening Ross Sea [Jacobs and Giulivi, 2010].

[4] Within this Pacific-Antarctic coastal setting, we describe the summer range of thermohaline properties observed near the GIS fronts from 1994 to 2011, focusing on 2000 and 2007 data sets that provide the best spatial coverage. The near-Getz observations are compared with similar measurements seaward of the ice shelf and near the Pine Island Ice Shelf (PIIS), and with yearlong records near the base of the thermocline off one of the GIS fronts. Vertical profiles of temperature, salinity, and dissolved oxygen permit calculations of water column meltwater content, geostrophic velocity, seawater, and meltwater transports to and from the sub-ice cavity, and estimates of ice shelf basal melting [Jenkins, 1999; Jenkins and Jacobs, 2008; Jacobs *et al.*, 2011]. Those melt rates are then set against independent results derived from satellite observations and firn modeling [Rignot *et al.*, 2013]. Most ocean measurements were acquired during February to March cruises of the research icebreaker *NB Palmer* and are available along with related information from [www.marine-geo.org](http://www.marine-geo.org). CTD/

O (conductivity temperature pressure/dissolved oxygen) data collection and reduction procedures are available from e.g., Jacobs *et al.* [2002], the National Oceanographic Data Center and [www.ldeo.columbia.edu/~claudiag/ASEP/](http://www.ldeo.columbia.edu/~claudiag/ASEP/). Atmospheric forcing on the regional ocean is inferred from the ECMWF ERA Interim reanalyses [Simmons *et al.*, 2006], <http://data.ecmwf.int/data>.

## 2. Ocean Properties Near the Getz

[5] Seawater profiling has typically been accomplished in open water along the coastline and in heavy sea ice near the continental shelf break. Casts were closer together in 2007 than in 2000, but are minimal or lacking at the narrow ice fronts flanking Carney Island (Figure 1). East of Siple Island a warmed 150–200 m surface layer probably related to the persistent Amundsen Polynya [Yager *et al.*, 2012] overlies a thick Winter Water (WW) temperature minimum (Figure 4a). West of there, warmer surface waters are missing and the cold WW layers are substantially thicker. Correspondingly deeper western thermoclines terminate above a wider range of bottom temperatures than at the eastern openings, and haloclines provide stability to both the WW and thermocline. On the shallower outer shelf, haloclines are weaker within the WW and stronger above and below it, ending in thin bottom boundary layers or intersecting the seafloor (Figure 4b). Some of those near-bottom layers will

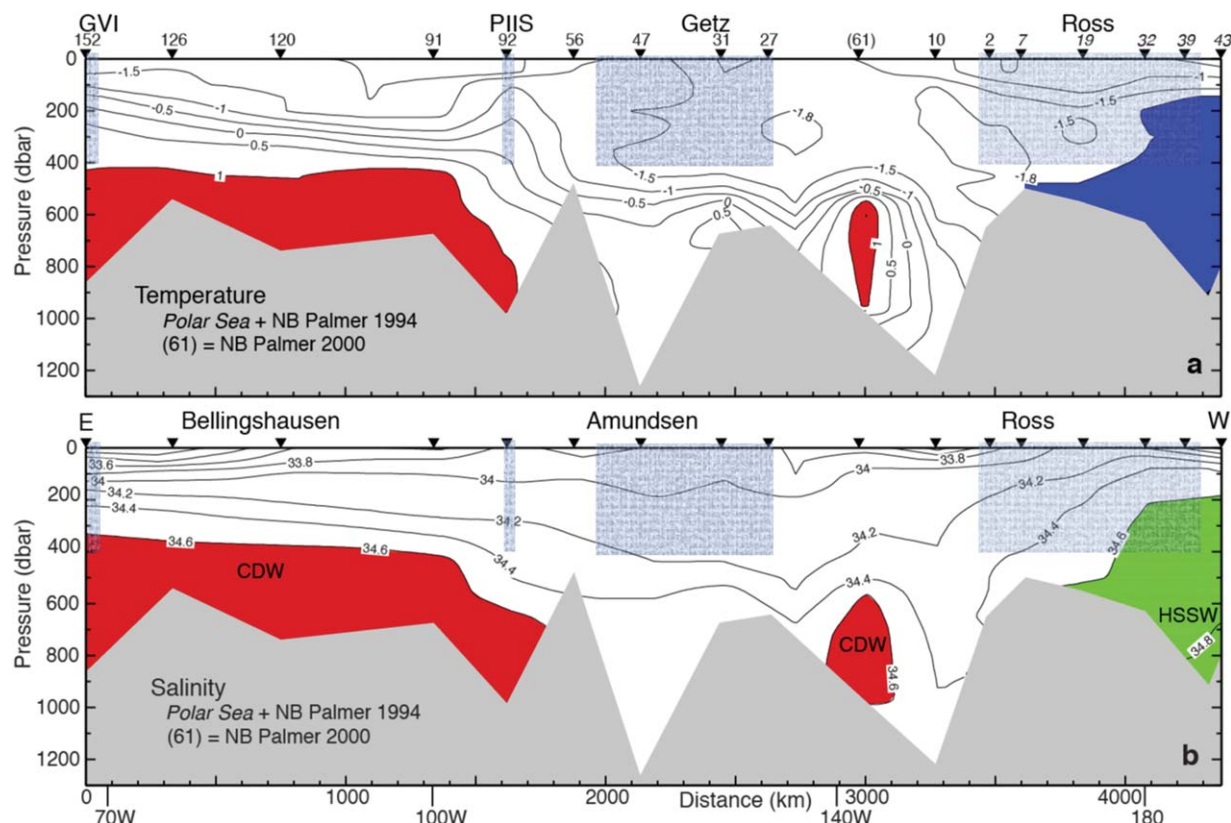


**Figure 2.** (a) Ocean temperature and (b) salinity along the Pacific-Antarctic coastline (Figure 1 inset) in late summer 1994. Contoured from 50 dbar  $\times$  270 km grids defined by the CTD casts shown, 5 February to 30 March 1994. Lightly shaded areas locate the George VI, Pine Island, Getz and Ross Ice Shelves. Circumpolar Deep Water (CDW;  $>1.0^{\circ}\text{C}$  and  $34.6$ ) occupies deep continental shelf regions east of the Getz, and intermittently as far west as CTD 10, represented here by CTD (61) on 28 January 2000. Cooler and fresher modified CDW (mCDW;  $<1^{\circ}\text{C}$  and  $34.5\text{--}34.6$  in Figure 5) prevails near the Getz coastline, and cold Shelf Water (HSSW;  $<-1.8$  and  $>34.6$ ) in the Ross sector. 1 dbar  $\sim$  1 meter.

feed mCDW into thicker pools in the deeper troughs along the Getz coastline (Figure 4a). Spatial variability of thermohaline properties, with density more closely tracking salinity in this environment, thus appears to be a significant aspect of ocean forcing on the GIS cavity.

[6] Temporal variability of ocean properties also has a large influence on the GIS, with shallower thermoclines and warmer mCDW near the ice fronts in 2007 than in 2000 (Figure 4a). For example, no profiles near 600 m were warmer than  $-0.5^{\circ}$  in 2000, but all were warmer in 2007 when a maximum of  $1.34^{\circ}\text{C}$  west of Siple Island was higher than any measured temperature through early 2009 in PIB. Many profiles display step-like structures up to tens of meters thick in the thermocline and WW, indicative of mixing processes that can include melt-induced layering near shelf ice [Jacobs *et al.*, 1981]. On the shallower outer shelf, thermoclines and upper/lower haloclines are steeper (Figure 4b) along with a few atypical profiles that suggest stronger variability near the shelf break. Close to those outer-shelf profiles, but on the upper continental slope, T/S properties at seven stations each year show a higher mCDW temperature maximum in 2007, and mostly fresher conditions along the deep water—surface water mixing line (Figure 4c). The symbols denote mean outer shelf properties near bottom at the Figure 4b sites, illustrating

both the temporal and cross-shelf break spatial differences between the two years.

[7] To broaden the temporal context, we average near-Getz profiles from each available year and show temperature relative to the in situ freezing point ( $T - T_f$ ) to illustrate the erosive capability of relatively isothermal mCDW at increasing depths (Figure 5). While averaging removes the small-scale variability and can introduce virtual structure (e.g.,  $>650$  m in Figure 5c), it simplifies comparisons between years and other ice shelves (dotted lines). The more complete 2000 and 2007 data sets encompass most of the sub-surface thermal range observed near the Getz over an 18 year period (Figures 5a and 5b). Near the eastern ice fronts, full upper water column warming during summer is indicated by the early-season single-station profiles (colored dashed lines), and temperature differences between 1994 and 2009 were much larger than near the PIIS (Figure 5a). Far-field temperatures in 1994 and 2007, also compared in Figure 3, tracked the freezing point near the Ross Ice Shelf and displayed much shallower thermoclines and warmer deep water in Marguerite Bay (Ryear and Myear in Figure 5c). Accompanying T/S diagrams for the GIS observations (Figures 5b and 5d) show the primary WW-mCDW mixing lines and their temporal shifts in relation to the density field. Those mixing lines bow more in 2007 than in

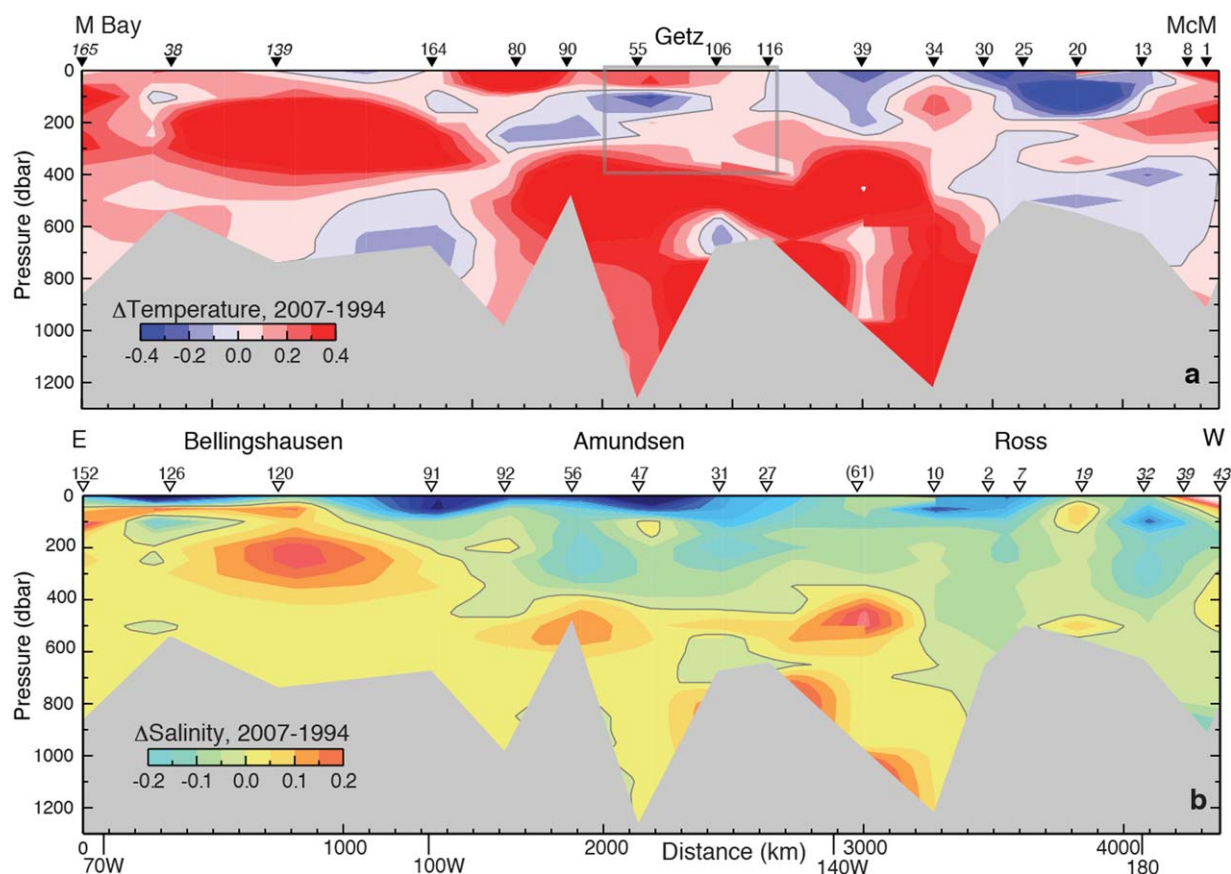


**Figure 3.** (a) Ocean temperature and (b) salinity differences near the Pacific-Antarctic coastline, 2007 – 1994, with the fields contoured as in Figure 2. In 2007, both properties were generally higher below surface layers in the Bellingshausen and Amundsen sectors, notably along the Getz Ice Shelf (gray rectangle). At shallower Amundsen and full Ross Sea depths the temperature differences were more variable, and salinities mostly lower in 2007. The CTD casts in 1994 and 2007 (open and solid triangles) were made from *JC Ross* in the Bellingshausen (8–30 March) and *NB Palmer* in the Amundsen and Ross sectors (3 February to 16 March). M Bay = Marguerite Bay; McM = McMurdo Sound.

2000 toward the black dashed lines that would characterize simple mixtures of mCDW and meltwater.

[8] Yearlong records of temperature, salinity, and pressure were obtained in the lower thermocline and upper mCDW on the western flank of the trough west of Wright Island (Figure 6). The filtered parameters reveal fortnightly tidal variability, masking shorter-term mooring tilt from intermittently stronger currents. Higher barotropic tidal amplitudes on the western than on the eastern Amundsen continental shelf (L. Padman, personal communication, 2008), in combination with rough bathymetry, could enhance mCDW mixing and upwelling throughout the Getz region. Temperatures range over  $\sim 0.3^{\circ}\text{C}$  and salinities over  $\sim 0.08$  near bottom (Figure 6a) and are positively correlated, suggesting the mCDW source region lies in the upper CDW, i.e., above the temperature maximum near the continental shelf break. Mean temperatures are closer to summer than winter extremes (Figure 6b), with an annual range less than the 2007 summer profile variability along the two eastern Getz fronts, and warmer than 2000 profiles at the same depth (black bars in Figure 4a). The colder, more widely ranging temperatures in the lower thermocline are highest in summer, implying that winter surface processes may perturb the lower

thermocline and upper mCDW at source locations. Seasonality does not dominate widespread deep temperature records on the SE Pacific-Antarctic continental shelf [Jacobs *et al.*, 2012; K. Assmann *et al.*, Variability of circumpolar deep water transport onto the Amundsen Sea continental shelf through a shelf break trough, submitted to *Journal of Geophysical Research*, 2013]. Less clear is whether vertical coherence in the temperature records indicates eddying deep water inflow, as on the west Antarctic Peninsula [Martinson and McKee, 2012] or barotropic fluctuations in a persistent baroclinic transport [Arneborg *et al.*, 2012]. In either case, these records show that mCDW had potential access to the GIS cavity during the winter of 2006, although at depths below most ice drafts (Figure 4d). With thermohaline ranges through 2006 similar to those on the summer 2007 CTD casts, annual ice shelf melt estimates based on summer profiling should not display a large seasonal bias.

### 3. Ice Shelf Melting

[9] Past work has shown that reasonable estimates of ice shelf basal melting can be derived from a composite of temperature, salinity, and dissolved oxygen tracers from

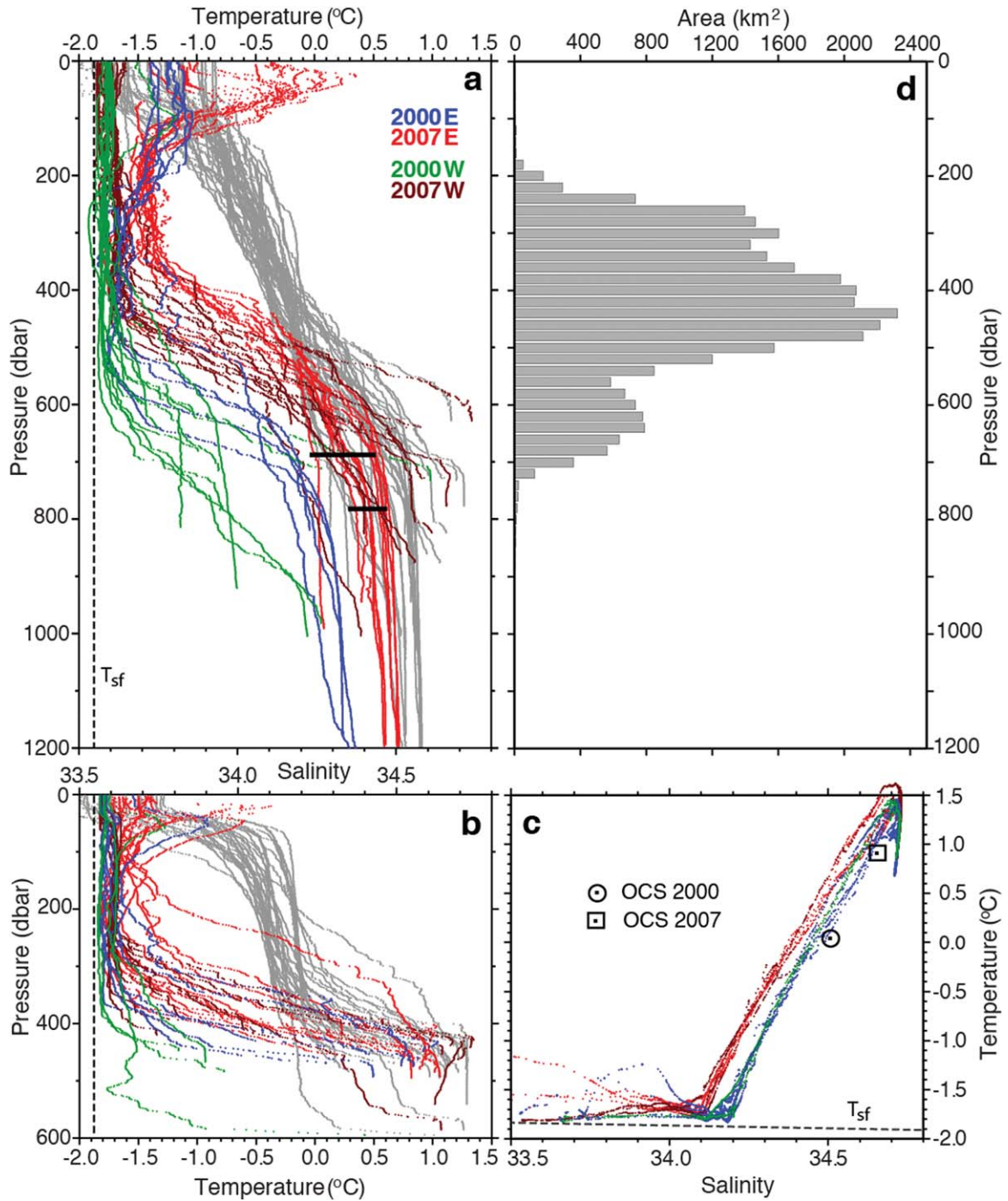


**Figure 4.** Temperature/depth (color) and salinity/depth (gray) profiles from the 2000 and 2007 (Figure 1) CTD stations along the (a) Getz ice fronts and (b) outer continental shelf. Siple Island divides these late summer (18 February to 11 March) Eastern and Western profiles. The black bars in Figure 4a indicate annual (2006–2007) temperature ranges at the mooring seaward of Wright Island (Figures 1 and 6).  $T_{sf}$  is the sea surface freezing temperature. Deep temperatures varied little below 1200 dbar (maximum 1473 dbar); surface salinities were below 33.5 at several stations east of Siple. (c) Temperature/salinity at 14 upper continental slope stations (976–1146 dbar) near the outer-shelf profiles in Figure 4b, with symbols showing average near-bottom T/S properties at 10 closely spaced outer continental shelf (OCS) stations from Figure 4b. (d) Getz Ice Shelf draft distribution from the Bedmap2 compilation [Fretwell *et al.*, 2013].

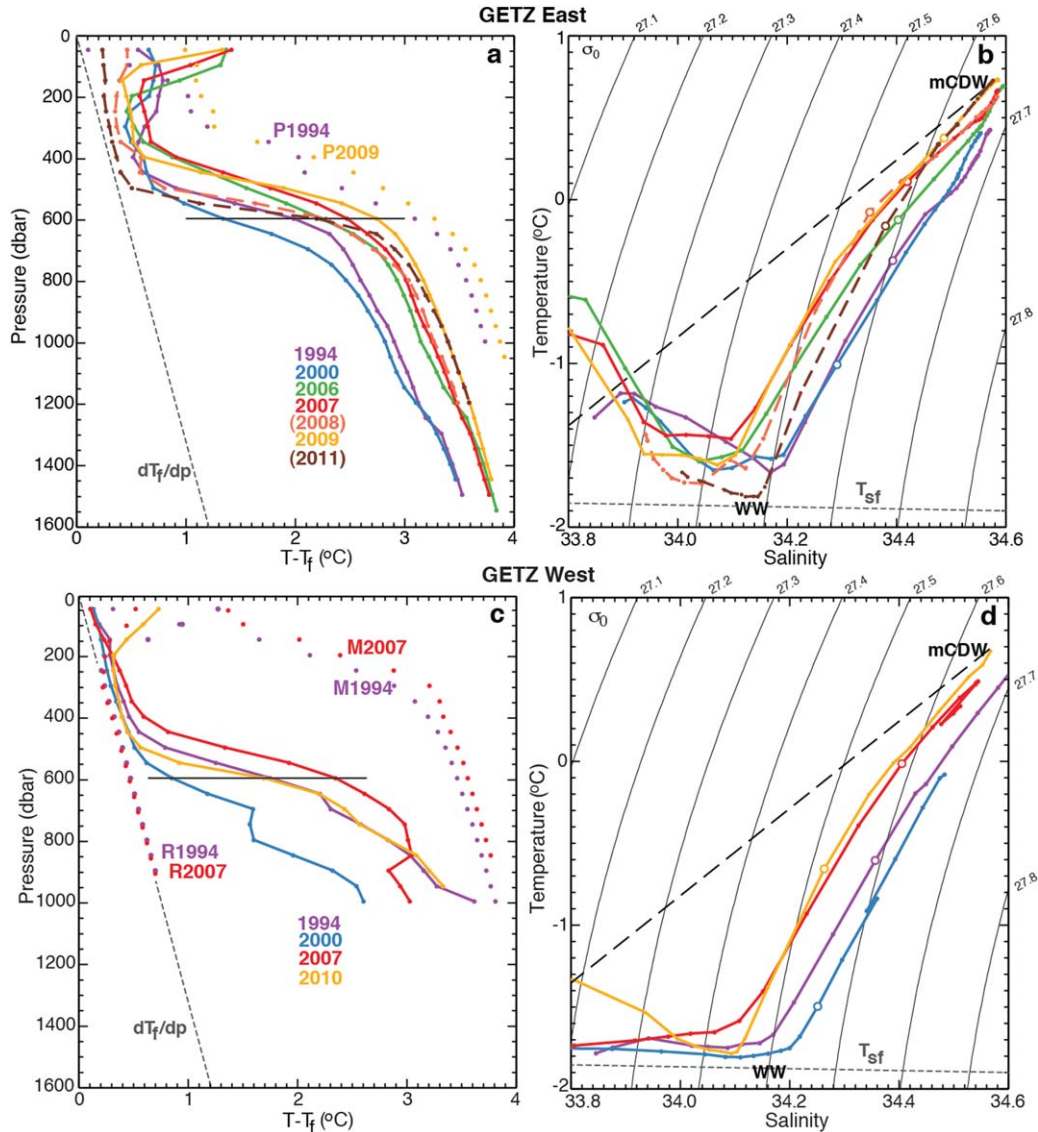


**Figure 5.** (a) Mean temperature above freezing ( $T - T_f$ ) profiles (colored solid lines) each summer near the eastern Getz ice fronts flanking Wright Island (Figure 1). Dashed lines are single profiles in December 2007 and 2010 (2008 and 2011 summers); colored dots (P1994 and P2009) are from CTD profiles near the Pine Island Ice Shelf (Figure 2). The in situ freezing point line ( $dT_f/dp$ ) illustrates the influence of pressure on the melting potential of nearly isothermal surface and deep waters (Figure 4). (b) Temperature/salinity diagram of the near-Getz profiles in Figure 5a, with density anomaly isopycnals. Open circles correspond to the 600 dbar values in Figure 5a. The (2009) mixing line between mCDW and ice shelf meltwater is dashed black. WW = Winter Water;  $T_{sf}$  as in Figure 4. (c) As in Figure 5a, but for profiles near the ice fronts west of Siple Island, near George VI Ice Shelf in Marguerite Bay (M1994 and M2007) and the Ross Ice Shelf (R1994 and R2007). (d) As in Figure 5b, but for the near-Getz profiles in Figure 5c.

CTD profiles near calving fronts, in relation to appropriate water mass end-member properties defined by the CDW, WW, and shelf ice [Jenkins, 1999; Jenkins and Jacobs, 2008; Jacobs *et al.*, 2011]. Combined with cross-frontal geostrophic transport calculations, the method assumes those property tracers characterize locally added ice shelf meltwater content, define exclusion depths above which surface contamination is likely, and represent year-round conditions. Application to the Getz Ice Shelf adds uncertainty because of its several ice front openings recessed between

islands, and irregular seafloor boundaries near which seawater can enter and exit the cavity. Limited observations at two small openings and irregular station positions in possibly narrow coastal flows raise additional concerns. On the other hand, the 2000 and 2007 CTD measurements cover  $>90\%$  of the ice front opening areas, span most of the 18 year thermohaline range in Figure 5a and are close enough in time that changes in cavity geometry from thinning or thickening ice should have a minor impact. The marked thermohaline differences between the two years thus

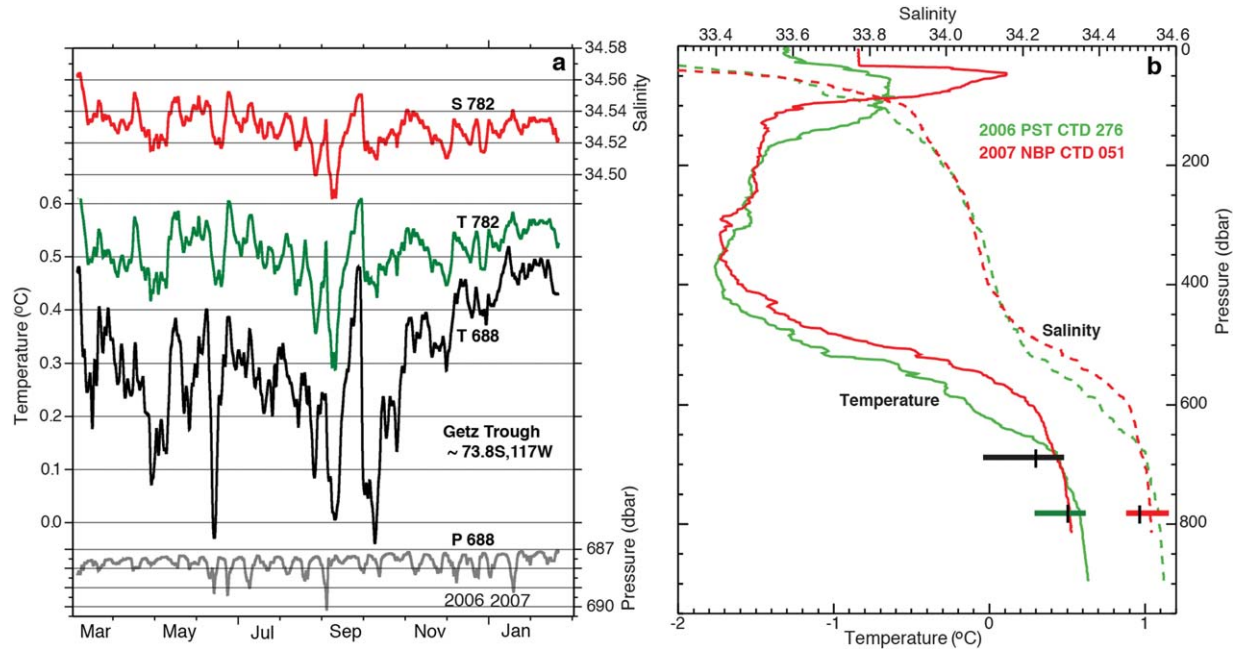


**Figure 6.** (a) Temperature, salinity, and pressure from 9 March 2006 to 21 February 2007 recorded by bottom anchored instruments at 688 and 782 dbar ( $\sim 3$  m above the seafloor) seaward of Wright Island (triangle in Figure 1). A 2 day low-pass filter has smoothed the records; unfiltered pressure excursions occasionally reached 5–10 dbar. (b) Time series depths, ranges and averages (tics on colored bars) from Figure 6a superimposed on nearby CTD profiles at the times of mooring deployment from the *Polarstern* and recovery from the *NB Palmer*.

provide an opportunity to assess the influence of temporal and spatial ocean variability on ice shelf melting.

[10] The GIS draft distribution from the Bedmap2 compilation [Fretwell *et al.*, 2013] extends to  $\sim 800$  m below sea level (Figure 4d). Comparing those drafts with the adjacent temperature profiles (Figure 4a), more basal ice would have been exposed to the shallower, warmer thermocline in 2007 than the deeper, cooler thermocline in 2000. Melting freshens, cools and lightens the seawater, making it sufficiently buoyant to reach the sea surface, or enabling mixing back into the pycnocline at levels set by ice draft and the modified seawater density [Jacobs *et al.*, 2011, 1981]. The latter case is more applicable to the GIS, and both the density fields and meltwater fractions at the Figure 4a sites were notably different in 2000 and 2007 (Figures 7a and 7b). The highest meltwater fractions in 2000, at a station directly east of Duncan Island, reappeared at that ice front opening in 2007, exceeding 15 mL/L (1.5%) at a depth near 150 m and the 27.3 density anomaly. Meltwater content was highest in 2007 along the eastern ice fronts, with maximum values near the 27.3 and 27.54 density anomaly surfaces. Mid-water column minima near 27.47 in 2007 and 27.54 in 2000 were similar to near-bottom (background) meltwater fractions. The PIB reference profiles display similar vertical structure, with 1994 and 2009 values intermediate between those at the western and eastern Getz ice fronts in 2000 and 2007. Mean temperature differences between the two years were largest around 27.54 (Figure 7c), corresponding to the  $\sim 450$ –600 dbar range and the upper thermocline and lower halocline in Figure 4a.

Density field changes reflected in thermocline depth and mCDW volume will likely influence basal melting under the Getz.

[11] Sections contoured from the Figure 4a profiles show the distribution of temperatures and salinities along the Getz ice fronts in 2000 and 2007 (Figures 8a and 8b, 9a, and 9b). The most striking temperature and salinity differences are the higher values in 2007 in the 400–800 m interval, i.e., in the depth range of the thicker ice in Figure 4d. In both years, near-bottom temperatures were similar and salinities much higher in the shallow trough directly west of Siple Island than in much deeper troughs east of Duncan Island, an indication that some flow within the cavity could be eastward. The dense mCDW will be renewed from below as melting increases seawater buoyancy and upwelling, accompanied by lateral circulations to and from the cavity at ice shelf draft depths. Meltwater fraction extremes are more sharply defined at depth and near the surface exclusion levels in 2007 (Figure 9c versus Figure 8c), and in both years could result in part from the melting of eastern Amundsen ice shelves and icebergs. Geostrophic velocity estimates based on adjacent CTD profiles are extrapolated into triangles along the seafloor (Figures 8d and 9d), but remaining gaps include the openings around Carney Island. Deep inflows (outflows) on the eastern (western) sides of most openings suggest clockwise circulations in sub-ice troughs, within which diffusion [Phillips, 1970] and melt-driven export above will favor upwelling within the cavity. Outflows appear stronger at the upper levels in 2007, and in some western lower water columns in 2000.

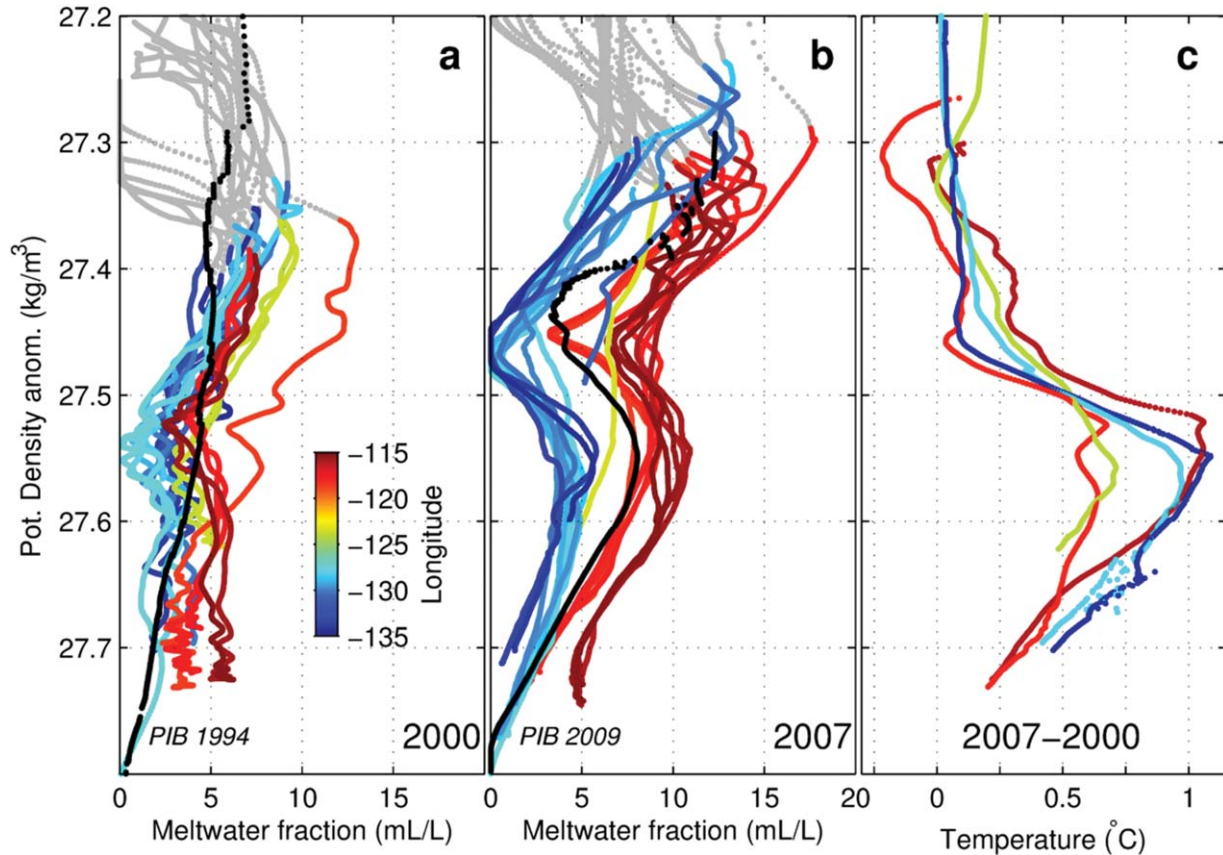


**Figure 7.** (a and b) Meltwater fraction profiles referenced to potential density near the Getz ice fronts in 2000 and 2007. From 25 m running averages color scaled by longitude and compared with mean Pine Island Bay profiles in 1994 and 2009 (black). The upper profiles (gray), some extending above 27.2, are in the zone of probable influence by sea surface fluxes, defined by a standard deviation threshold between meltwater estimates in T/S, T/O<sub>2</sub>, and O<sub>2</sub>/S space [Jenkins, 1999]. (c) Mean temperature differences, 2007 – 2000, at the five largest ice front openings, with the same density and color scaling.

[12] Seawater transport into the Getz cavity each year for six ice front (gate) combinations and surface exclusion zones averaged 79% higher in 2007, leveraging meltwater exports substantially higher than in 2000 (Tables 1 and 2). Parallel estimates comparing meltwater inflow and outflow would ideally give the same result, the differences reflecting possible error sources noted above and in the velocity adjustments imposed to achieve mass and property balances. Overall ice equivalent differences exceed the  $1\sigma$  uncertainty range and average 3.7 times larger in 2007, consistent with the warmer conditions, shallower thermoclines and stronger circulation that year. While full budget closure was not realistically achieved with more than four gates, sampling was sufficient to compare fluxes through the five main openings (Table 3). Net transports through each opening relative to its 27.47 isopycnal were more coherent in 2007, with strong deep inflows (outflows) west (east) of Siple Island. With two exceptions that pattern is the same in 2000, and outflows above 27.47 prevailed at 80% of the openings each year. Upwelling within the cavity relative to that isopycnal (sum in Table 3) was 3.4 times stronger in 2007, similar to the greater meltwater production that year. Combining the estimates in Tables 1 and 2 ( $137 \pm 16 \text{ km}^3$  of basal ice melting in 2007 and  $37 \pm 13 \text{ km}^3$  in 2000) over an area of  $33,395 \text{ km}^2$  corresponds to

areal mean rates of  $4.1 \pm 0.5$  and  $1.1 \pm 0.4 \text{ m a}^{-1}$ . Those rates are lower than a  $6.2 \text{ m yr}^{-1}$  rate estimated from ocean temperature [Shepherd *et al.*, 2004] but with a spread sufficient to demonstrate the strong influence of temporal and spatial ocean variability on ice shelf basal melting.

[13] The basal melt rates derived from these late summer data sets are  $\sim 4$  times higher in 2007 when the adjacent ocean was warmer and its circulation stronger than in 2000. Both estimates may be low, since meltwater is not accounted for in the near-surface exclusion zones, the narrow gaps between some islands, or in boundary transports that closely track the rough bathymetry. Lower rates (not shown) from geostrophic calculations restricted to depths above the maximum ice shelf draft suggest some downward mixing of meltwater by tidal motion and freezing. Our melt rates are comparable to numerical ocean modeling results of  $2\text{--}5.4 \text{ m a}^{-1}$  [Hellmer, 2004; Timmermann *et al.*, 2012]. Higher estimates of  $8\text{--}23 \text{ m yr}^{-1}$  have included simulations with and without tides and a wide range of ice shelf areas [Olbers and Hellmer, 2010; Schodlok *et al.*, 2012; Robertson, 2013]. We are unaware of any ocean model that has focused exclusively on the Getz.

[14] An independent method of estimating ice shelf basal melting combines ice motion from satellite radar interferometry, ice thickness and its changes from satellite laser

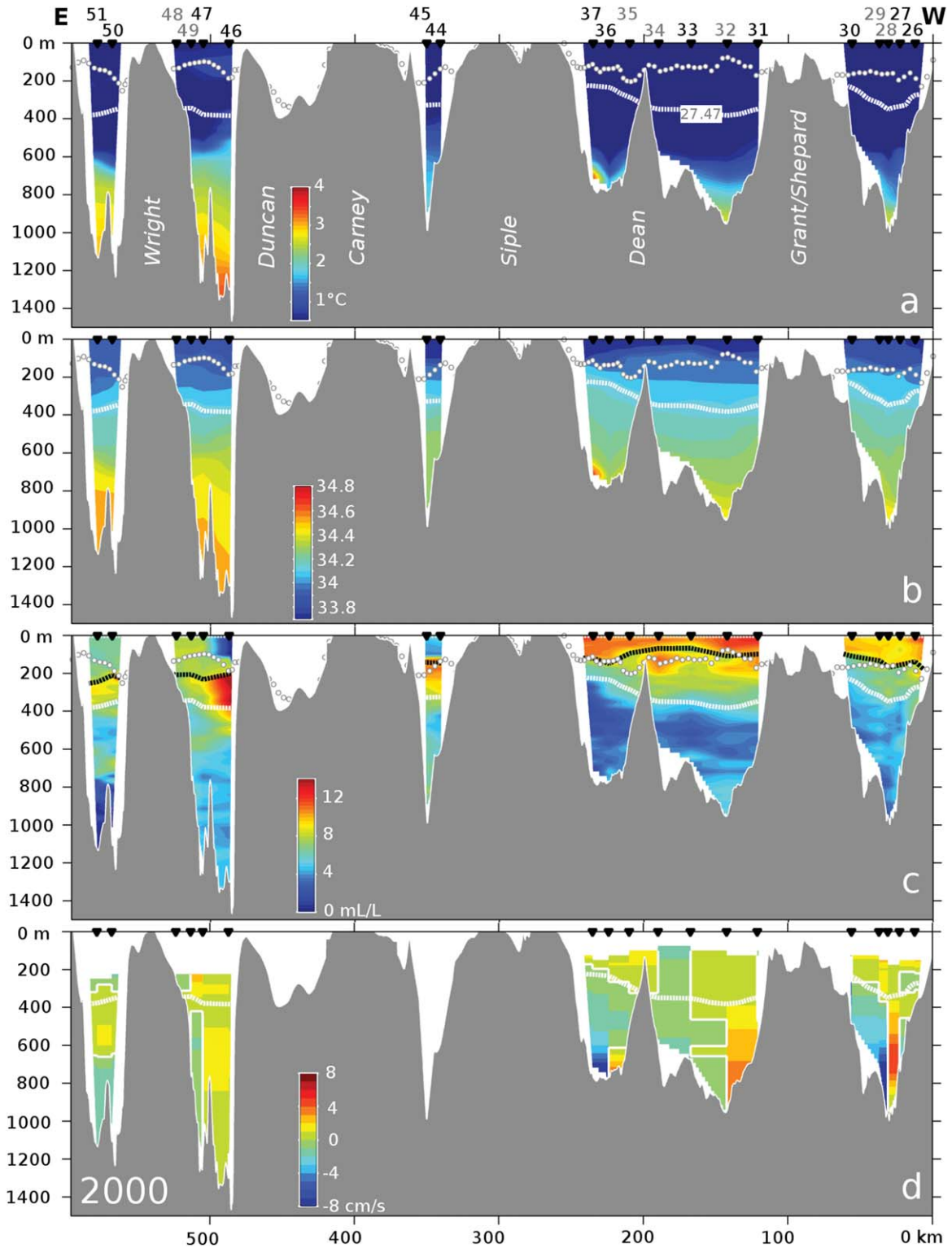


**Figure 8.** (a) Temperature above freezing, (b) salinity, and (c) meltwater fraction derived from gridded ( $1 \text{ km} \times 25 \text{ m}$ ) fields of CTD profiles 26–51 along the Getz ice fronts in 2000, and (d) geostrophic velocity with outflows positive (warmer colors). White dashed lines show the surface-referenced 27.47 potential density anomaly, closer to mean ice shelf depths (Figure 4) than the shallow near-ice front drafts (white dotted lines). Minimum velocity adjustments to achieve mass and property balances shift an initial reference level at the mid-water column meltwater minimum (Figure 7) to the white lines in Figure 8d. Black dotted lines in Figure 8c show standard exclusion depths above which surface contamination is likely.

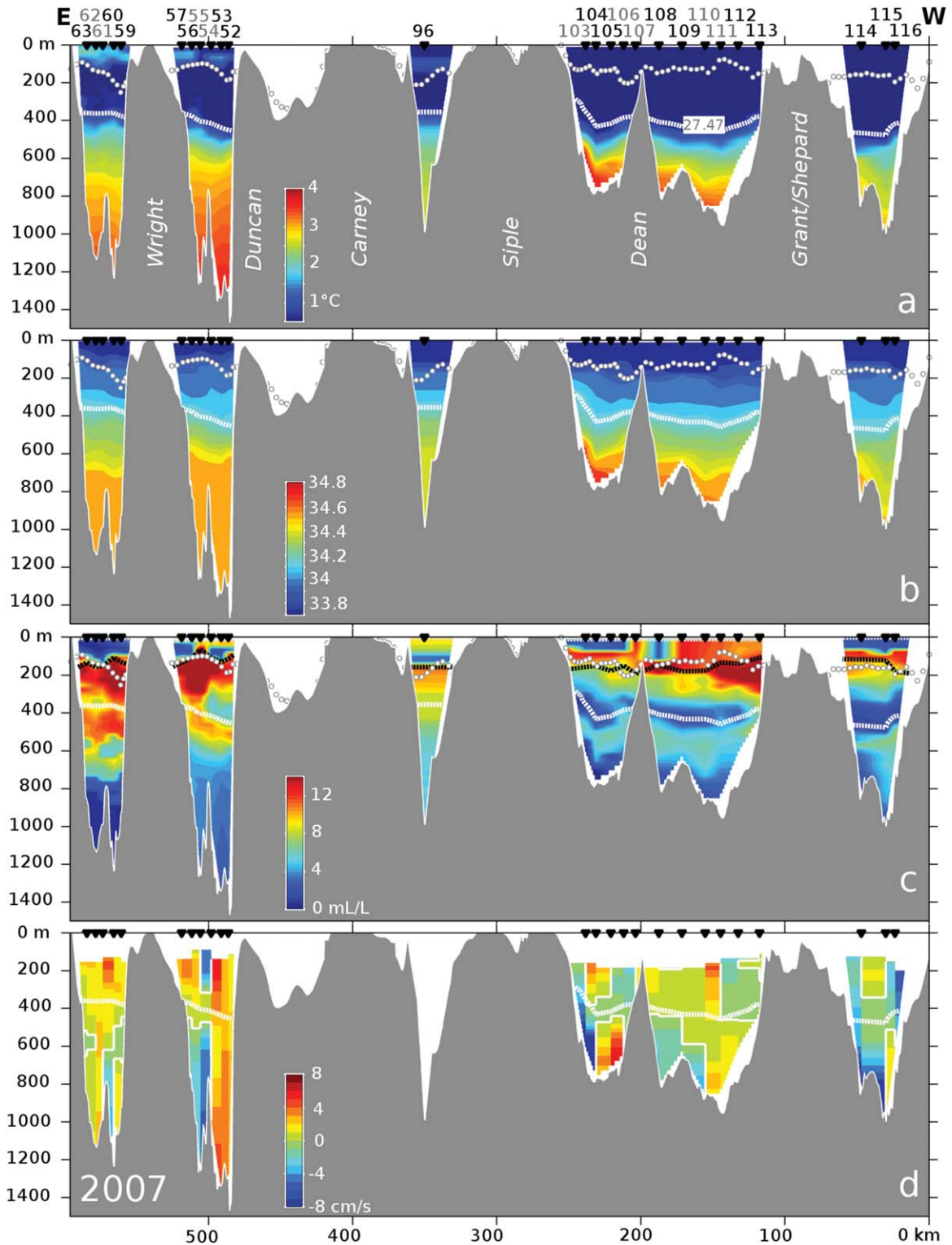


Figure 9. As in Figure 8, but contoured from 2007 CTD profiles 52–116.

altimetry, and modeling of the surface firn layer [Rignot *et al.*, 2013]. For the GIS that investigation found steady state and actual ice equivalent area-average melt rates of  $2.5 \pm 0.2$  and  $4.6 \pm 0.4$   $\text{m a}^{-1}$  of ice in 2007–2008 (Figure 10). The difference is the thinning rate, based on 2003–2008 satellite data, comparable to  $2.0 \pm 0.4$   $\text{m a}^{-1}$  for the same period [Pritchard *et al.*, 2012],  $\sim 2.3$   $\text{m a}^{-1}$  from

1992 to 2001 over the eastern and western Getz [Zwally *et al.*, 2005] and  $\sim 1.8$   $\text{m a}^{-1}$  from 1994 to 2008 over  $\sim 75\%$  of the GIS area [Shepherd *et al.*, 2010]. Sectional thinning rate differences in studies where the ice shelf has been sub-divided suggest flow within the cavity between its ice fronts, consistent with the Table 3 transports, and with gaps south of the pinning islands in Figure 10. The indirect

**Table 1.** Seawater and Meltwater Transports Beneath the Getz Ice Fronts for Various Combinations of Openings (Gates) and Surface Exclusion Zones in 2000<sup>a</sup>

Number of Openings	Surface Exclusion	Seawater Transport (mSv)			Melt Transport (km <sup>3</sup> yr <sup>-1</sup> iceq)		Max (Mean) Correction (cm s <sup>-1</sup> )
		In (mSv)	Diff (mSv)	Diff (iceq) (km <sup>3</sup> yr <sup>-1</sup> )	In	Diff	
4	Standard	-956	0.84	29.7	-138.9	56.8	10.9 (0.9)
	$\sigma > 27.31$	-1014	0.75	26.3	-151.7	57.3	12.8 (0.9)
3	Standard	-909	0.51	17.8	-137.7	49	1.1 (0.2)
	$\sigma > 27.31$	-1071	0.86	30.5	-176.4	40	12.3 (1.1)
2	Standard	-1069	0.81	28.7	-179.4	30.2	2.6 (0.8)
	$\sigma > 27.31$	-1041	0.98	34.5	-171.9	41.1	1.2 (0.4)
Overall Estimates				Diff (iceq) = 27.9 ± 5.6		Diff = 45.7 ± 10.6	6.8 ± 5.7

<sup>a</sup>Standard and  $\sigma > 27.17$  or 27.31 exclusions refer to depths and isopycnals above which individual tracers diverge due to surface contamination. The Grant and nearby Shepard Islands are ignored in the 4-gate simulation, along with Dean Island for 3 gates and Wright Island for 2 gates (Figure 1). Geostrophic velocity adjustments for mass and property balance (last column, least squares) also help to compensate for short-term dynamic changes. Out-flow (not shown) + In = Diff. Seawater and meltwater fluxes in mSv ( $10^3 \text{ m}^3 \text{ s}^{-1}$ ) and km<sup>3</sup> of ice.

method error bar overlaps the uncertainty range of the 2007 rate from geostrophic calculations and meltwater tracers ( $4.1 \pm 0.5 \text{ m a}^{-1}$ ) and, in combination with the earlier thinning estimates, supports our inference that the low 2000 rate resulted from atypical ocean conditions and atmospheric forcing. Average basal melting is less consequential than its distribution because of the greater influence of melting near grounding lines on glacier inflow [Rignot and Jacobs, 2002; Jenkins et al., 2010; Schoof, 2010]. Both the balance and actual melt rates are higher there in Figure 10, reaching maxima of  $\sim 26 \text{ m/yr}$  near 74.78 S, 124.21 W, while freezing maxima of  $\sim 3\text{--}6 \text{ m/yr}$  occurred near the ice front at 74.52 and 133.43 W.

[15] The deep WW layers west of Siple Island (Figure 4a) included a 2000 profile with temperatures below the sea surface freezing point that had earlier suggested basal freezing under the GIS. Such Ice Shelf Water is more commonly found near the larger, cold-cavity ice shelves, and results from melting into cold, salty shelf water, followed by upwelling and freezing at lower pressures. High-salinity shelf waters are not formed in or transported to the Amundsen Sea, but lighter WW appears available to the GIS cavity year round (Figure 4). Along with warmer inflows, this water has the potential to lose enough sensible heat to basal melting to form marine ice. Basal freezing under the western Getz is confirmed by the negative melt rate distributions in Figure 10, especially in steady state. With comparable ice flux and surface accumulation, the freezing areas and rates would have been even greater in the colder 2000 environ-

ment when net melting was below that required for overall ice shelf mass balance. Cold ocean conditions also characterized PIB in early 2000, and more recently [Jacobs et al., 2011; P. Dutrieux et al., Strong sensitivity of Pine Island ice shelf melting to climatic variability, submitted to *Science*, 2013] probably lowering PIIS melting below its (2007–2008) steady state value of  $\sim 74 \text{ km}^3/\text{yr}$  (from 68 Gt/yr water equivalent in Rignot et al. [2013]).

#### 4. Ocean Properties and Circulation North of the Ice Shelf

[16] Having compared temperature and salinity profiles along the GIS with those near the continental shelf break (Figure 4), we next show temperature along sections that link the latter region with the eastern and western ends of the ice shelf in 2000 and 2007 (Figure 11). The volume of mCDW with  $T - T_f > 1.5^\circ$  (e.g.) decreases westward in each year, as it does along the ice fronts in Figures 8 and 9. The southward deepening of isotherms and a representative isopycnal are consistent with the expected presence of a westward coastal current. Paired outer-shelf stations at ten Figure 11 sites averaged  $0.86^\circ$  warmer and 0.155 saltier near bottom in 2007 (OCS symbols, Figure 4c). That temperature increase exceeds any possible 7 year warming of the source CDW, but stronger upwelling over the continental slope in 2007 would have enabled deep water access to the continental shelf. Enhanced at shelf-break depressions and funneled southward in seafloor troughs, as modeled by

**Table 2.** As in Table 1, But for 2007

Number of Openings	Surface Exclusion	Seawater Transport (mSv)			Melt Transport (km <sup>3</sup> yr <sup>-1</sup> iceq)		Max (Mean) Correction (cm s <sup>-1</sup> )
		In (mSv)	Diff (mSv)	Diff (iceq) (km <sup>3</sup> yr <sup>-1</sup> )	In	Diff	
4	Standard	-1762	4.5	158.9	-293.7	133.2	4.1 (1.1)
	$\sigma > 27.17$	-2017	3.8	135.6	-359.1	131.4	5 (1.5)
3	Standard	-1658	4.27	150.4	-298.1	125.5	2.8 (0.9)
	$\sigma > 27.17$	-1790	3.57	125.9	-332.4	127.7	3.6 (1.2)
2	Standard	-1674	5.33	187.8	-307.9	123.4	1.7 (0.7)
	$\sigma > 27.17$	-1916	3.73	131.6	-368.4	113.6	2 (0.9)
Overall Estimates				Diff (iceq) = 148 ± 22.9		Diff = 125.8 ± 7	3.2 ± 1.3

**Table 3.** Net Seawater Transports In and Out (Positive) of the Five Largest Getz Cavity Ice Front Openings in 2000 and 2007, Above and Below the 27.47 Density Anomaly, Summed at the Right<sup>a</sup>

Year	Isopycnal	E < Ice Front Seawater Transport (mSv) > W					Sum
2000	<27.47	-27	13	29	47	2	64
2000	>27.47	6	128	-214	64	-46	-62
2007	<27.47	117	117	93	28	-137	218
2007	>27.47	158	407	-246	-141	-391	-212

<sup>a</sup>The Duncan-Carney-Siple Island complex separates the two eastern (3rd and 4th columns) from the three western openings (Figure 1). Standard deviations exceed 6 (1) of the ten values in 2000 (2007).

*St-Laurent et al.* [2013], e.g., that access may also be limited by sills on the outer shelf.

[17] Flows into and out of rectangular boxes defined by the loop and ice front sections are in the same directions both years (Figure 11, middle plot insets). Mostly stronger in 2007, transports (not shown) are persistently westward above and southward or eastward below the plotted reference isopycnals. Flows of 1010 and 1803 mSv into the GIS cavity in 2000 and 2007 are greater than those across the continental shelf break (658 and 1219 mSv), in part due to unadjusted imbalances resulting from locally stronger currents in the troughs and on the outer shelf. Net eastward flows across the eastern N-S sections (Figure 11, left) fit the southeastward trajectory of mCDW at the outer end of the trough that leads to the Dotson and eastern Getz ice shelves [Wahlin et al., 2010; Arneborg et al., 2012]. Continuation of that east-banked inflow would take it toward the Dotson, directly east of Martin Peninsula in Figure 1. While branches of that trough also extend beneath the eastern Getz cavities, net outflows occur at their deeper levels (Table 3), and seem likely to dominate the western flank time series records (Figure 6).

[18] Atmospheric forcing on the western Amundsen Sea north of the GIS can be roughly estimated from the 0.67° Lat/Lon ERA Interim reanalysis, from which we derived Ekman transports and pumping (Figure 12). A zonal wind stress minimum between easterly and westerly winds moves northward from winter to summer, averaging ~200 km north of the continental shelf. In 2000 (2007) that divergence was up to 100 km south (north) of the longer-term summer (JFM) average. The continental shelf break region seaward of the GIS is thus more often influenced by easterlies, whereas westerlies typically dominate lower-latitude shelf breaks, including the eastern Amundsen sector (Assmann et al., submitted manuscript, 2013; Dutrieux et al., submitted manuscript, 2013). A flow convergence appears near Siple Island in both summers, and transports increase more strongly southward from the off-shelf divergence in 2007. Transport differences show slightly stronger JFM upwelling north of the continental shelf in JFM 2007, although JFM 2000 is not anomalous over the 1979–2011 interval. A 2007/2000 ratio of 1.4 for southward transport between 72.67° S and 72.0° S in Figure 12 is similar to the net cross-shelf break transport in Figure 11. That is generally consistent with more mCDW above shelf-break depths and on the continental shelf in 2007. Stronger wind driven or tidal flows near the rougher shelf-break bathymetry off Siple Island could enhance eddy generation over the upper continental slope, intermittently provisioning the trough directly to its west with warm deep water (Figures 1 and 9).

As in *Klinck and Dinniman* [2010] such inferences are subject to reanalysis accuracy, the probable damping of momentum transfer by sea ice, and the time/space integration intervals over highly a variable domain.

[19] Ocean-ice studies in the Bellingshausen Sea have led to suggestions that stronger winds, vertical mixing, and variable sea ice cover on that continental shelf can modulate CDW heat flux to its ice shelves [Holland et al., 2010; Dinniman et al., 2012; Padman et al., 2012]. *Dinniman et al.* [2012] inferred less deep water sensitivity to surface processes in the Amundsen where it is lower in the water column (Figure 5c), perhaps in accord with the haloclines in Figure 4a. Accompanying temperature profiles could imply winter overturning down to the thermocline, however, and *Assmann et al.* [2005b] modeled a sea ice growth maximum in 1999 and net export from this sector. From 1979 to 2009, the northern sea ice edge at GIS meridians was farthest north in 1998 to early 2000 (225–245°E in *Comiso et al.* [2011]), consistent with stronger northward transports north of ~70°S in Figure 12. *Hall and Visbeck* [2002] associated a more positive Southern Annular Mode (SAM) index with an increase in upwelling around the Antarctic coast, compensating an enhanced northward Ekman drift in the surface waters. A measure of mid to high-latitude sea level pressure (SLP) differences, and generally more positive over recent decades, the SAM is overlain if not overwhelmed by ENSO-related processes in the Amundsen sector (E. Steig, personal communication, 2013). The period leading up to the early 2000 measurements was characterized by an unusually strong La Niña, e.g., and anomalously low SLP near 75°S, 130°W [*Stammerjohn et al.*, 2008]. With a less-positive SAM in the months prior to our 2007 measurements ([www.antarctica.ac.uk/met/gjma/sam.html](http://www.antarctica.ac.uk/met/gjma/sam.html)), the upwelling difference shown in Figure 12 is oppositely timed from what might be expected. The indices are zonal surface averages, however, and tropical teleconnections to this region have mainly shown changes in the atmosphere and sea ice extent well north of the Getz continental shelf. Coupled sea ice-air high-resolution modeling that can reproduce the range of ocean properties reported here could help to determine the roles of variable wind forcing and sea ice cover in deep water access to the GIS.

## 5. Summary

[20] Getz is the largest ice shelf along the SE Pacific-Antarctic coastline, with drafts ranging from ~100 to 800 m, a contiguous area of 33,395 km<sup>2</sup>, and calving fronts pinned by several large and small islands. Occupying the

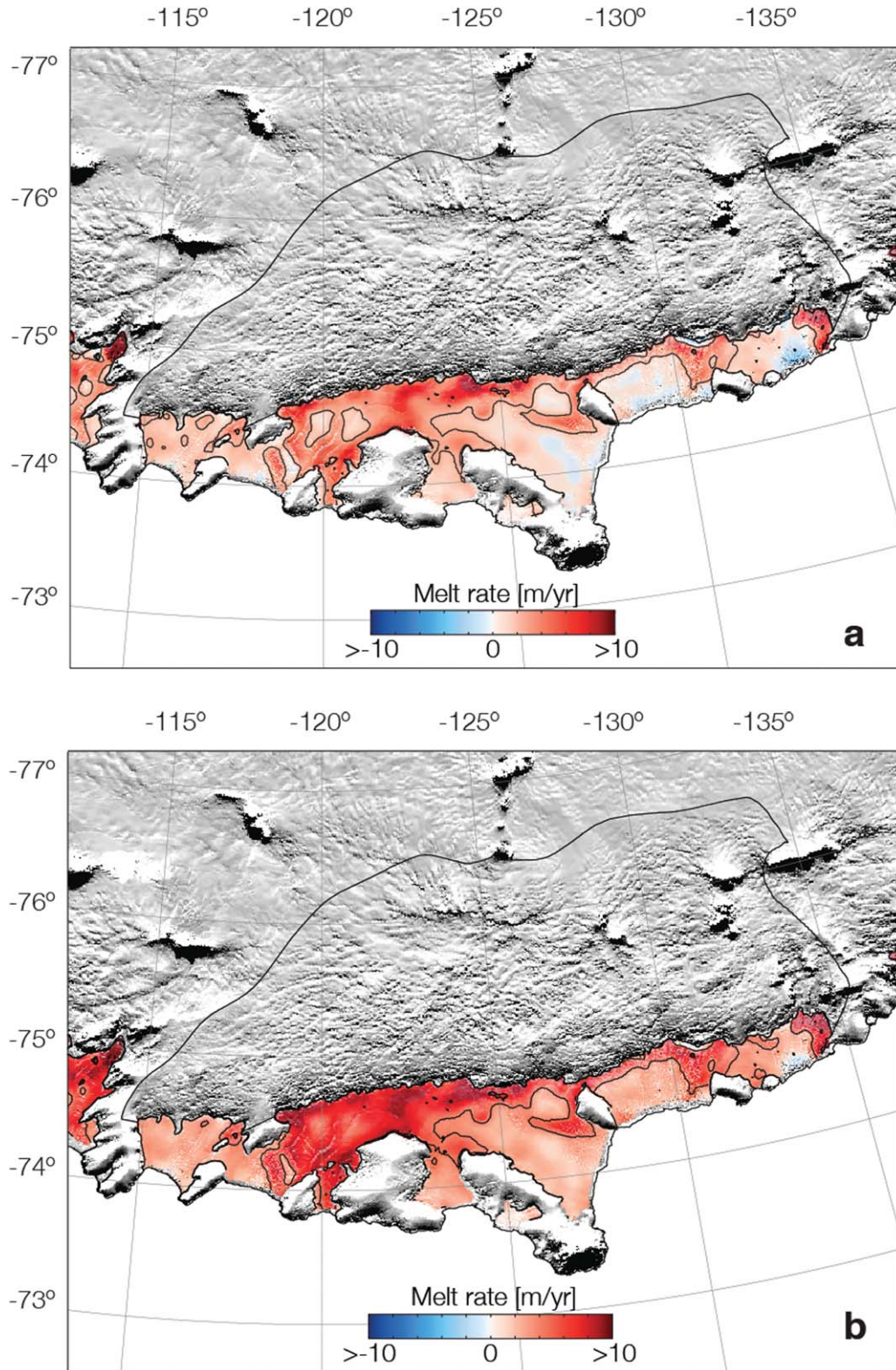


**Figure 10.** (a) Steady-state basal melt rate of the Getz, derived by combining 2007–2008 ice motion and ice front positions ( $\pm 150$  m) from satellite radar interferometry [Rignot *et al.*, 2011b], 2009 ice thickness and area from Bedmap2 [Fretwell *et al.*, 2013], and 1979–2010 mean surface mass balance from RACMO-2 (Regional Atmospheric Climate Model-2) [Lenaerts *et al.*, 2012] at a resolution of 10 km. (b) Actual melt rate distribution, with Figure 10a adjusted by ice shelf thickness change derived from corrected 2003–2008 ICESat-1 altimetry and firn data, after Pritchard *et al.* [2012] and Rignot *et al.* [2013]. The black line on the MOA2009 ice sheet delineates the 95,089 km<sup>2</sup> ice shelf drainage basin on MODIS imagery. Grounding line positions are from 1996 [Rignot *et al.*, 2011a]. Melt rates assume an ice density of 0.917, with contours at the average steady state and actual melt rates of 2.5 and 4.6 m/yr of ice.

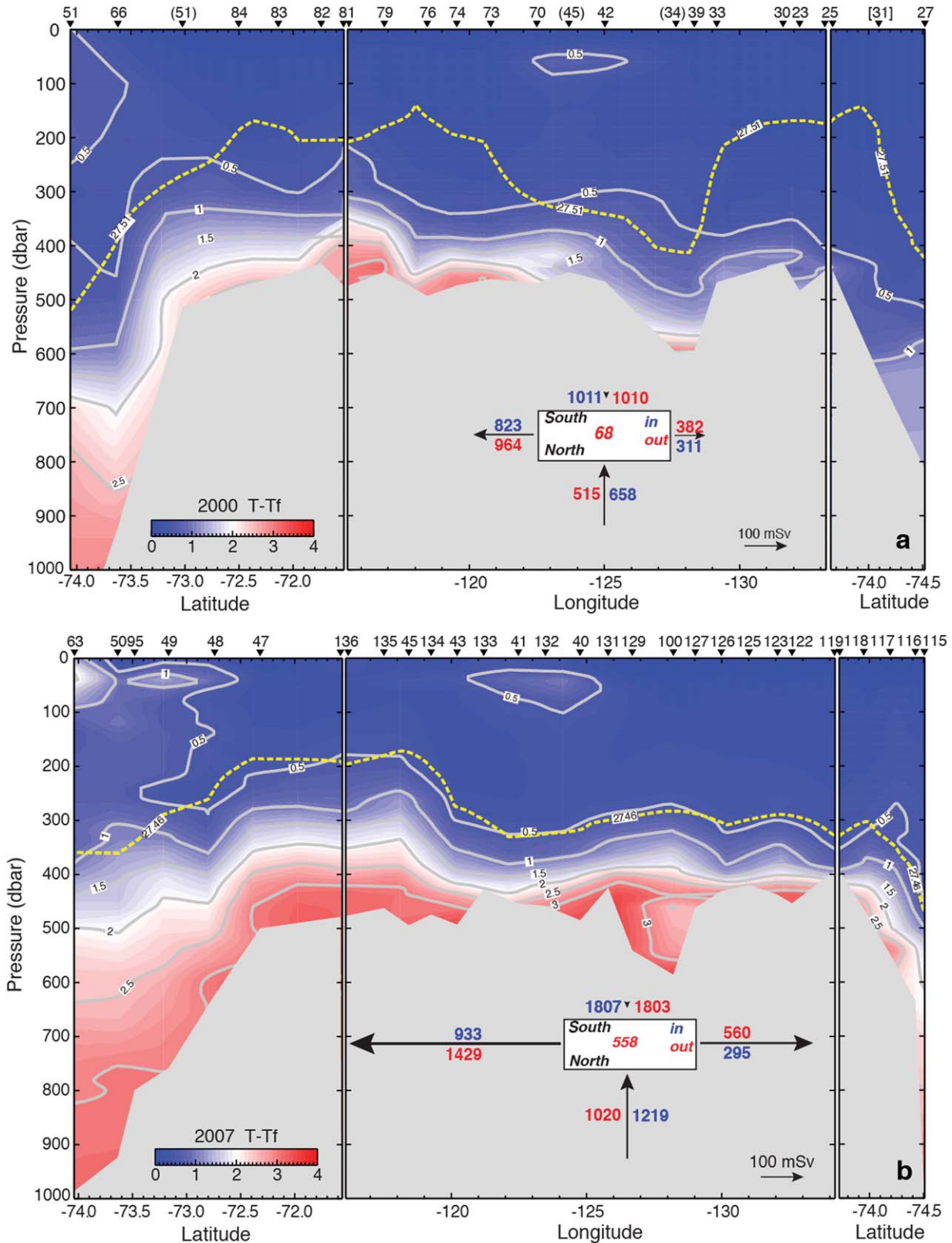


**Figure 11.** Temperature above freezing in (a) 2000 and (b) 2007 on sections around closed loops connecting the eastern and western (left and right) ends of the Getz Ice Shelf with a center panel transect along the continental shelf break (Figure 1). Rectangular inserts show geostrophic transports (in  $\text{mSv} = 10^3 \text{ m}^3 \text{ s}^{-1}$ ), referenced to the yellow-dashed isopycnals, into (blue) and out of (red) the region defined by these sections and by the ice fronts (from Tables 1 and 2). Arrow lengths are proportional to in/out transport differences, unadjusted overall and larger in 2007. The 2000 section is from 13 January to 11 March CTD profiles, with [31] shifted westward, supplemented by (34, 45, 51) from 24 February to 2 March 1994. Section (b) from 18 February to 11 March 2007.

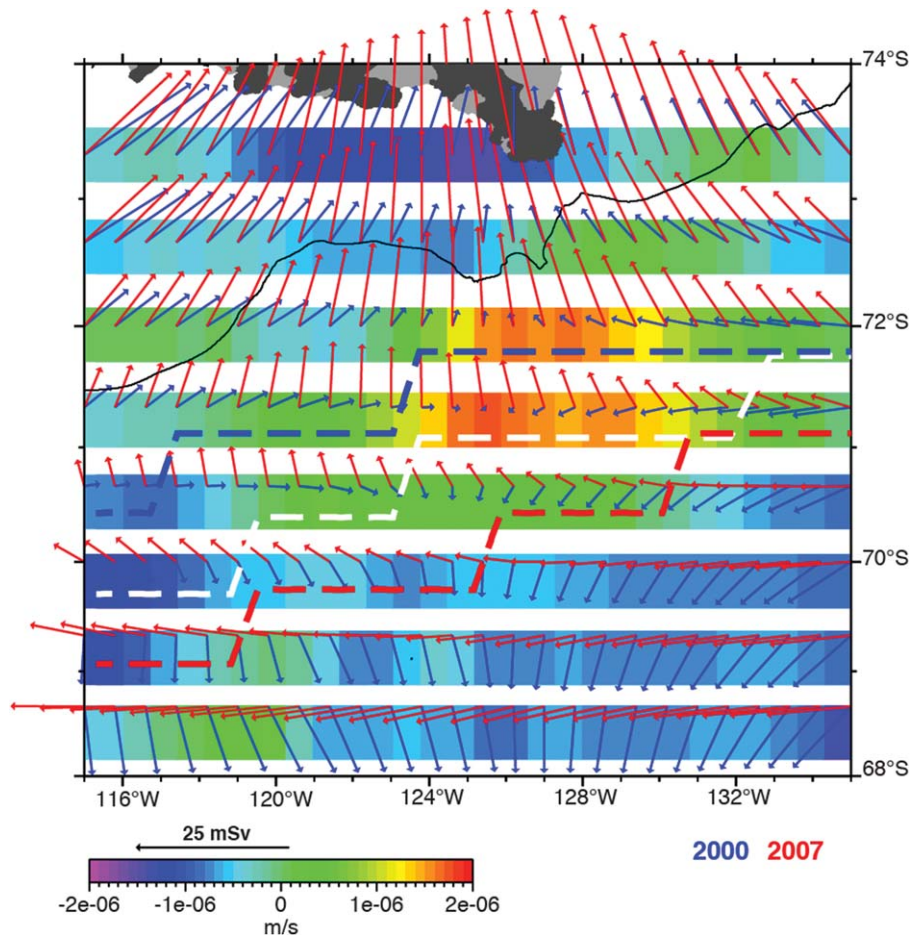


**Figure 12.** Atmospheric forcing on the sea surface/sea ice north of GIS, from the ERA Interim reanalysis wind stress. The blue (red) arrows indicate mean Ekman transports for JFM in 2000 (2007), and the background colors show upwelling differences (2007 – 2000). Dashed lines indicate JFM zonal wind stress minima in 2000 (blue), 2007 (red), and all months 1979–2011 (white). Siple Island is at top center, and the solid black line marks the 1000 m isobath on the upper continental slope (Figure 1).

southern quarter of a 100–350 km wide continental shelf, the seafloor along its coastline is characterized by glacially cut troughs that shoal seaward and toward ice cavity grounding lines. Summer temperature and salinity measurements from 1994 to 2010 show the GIS is subject to more changeable oceanic forcing than ice shelves in the Bellingshausen and Ross Seas. CTD profiling along the GIS revealed larger spatial variability in deep water properties during late summer than recorded during a full year at a mooring site near one of its ice fronts. Beneath cold surface waters, the thermocline was  $\sim 200$  m shallower in 2007 than in 2000, indicative of shifting access of deep water to the continental shelf and ice shelf base. Water column meltwater content, typically  $< 1.5\%$  from temperature, salinity, and dissolved oxygen tracers, was also higher in 2007. Geostrophic velocities adjusted for budget closure and excluding near-surface zones of probable tracer contamination yield seawater transports of  $\sim 1.0$  and  $1.8$  Sv to and from the GIS cavity in 2000 and 2007, along with meltwater transports corresponding to area-average basal melt rates of  $1.1$  and  $4.1$   $\text{m a}^{-1}$  of ice. Independent calculations from satellite measurements and firm modeling give steady state and total melt rates of  $2.5$  and  $4.6$   $\text{m/yr}$  of ice in

2007–2008. At the lower 2000 rate the GIS would have been thickening, apparently due to anomalous atmospheric forcing. The higher 2007 geostrophic and glaciological melt rates are consistent with earlier remote sensing estimates of  $\sim 2$   $\text{m/yr}$  thinning, but lower than most ocean circulation modeling results. In comparison with other ice shelves [Rignot *et al.*, 2013], the 2007 melt rates made Getz the largest source of ice shelf meltwater in the Southern Ocean at that time.

[21] Remote sensing methods and topside accumulation modeling can now integrate the distribution of ice shelf basal melting over space and time. The high spatial and temporal variability of ocean properties and circulation near the GIS combined with the difficulty of reaching it by ship constrain the regular use of CTD/O profiling for monitoring ice shelf response to ocean change. Sporadic in situ observations and moored time series records can furnish essential validation data for glaciological methods and ocean modeling, however, along with baselines and reference points for future studies. GIS melt rates are clearly sensitive to ocean temperature, thermocline depth, circulation strength, bathymetry, and ice thickness. Continued 2007-level ocean forcing and ice thinning would eventually slow

the melt rate, as would more frequent conditions like those observed in early 2000. Continued stability of the Getz depends on how changes in the winds and sea ice cover influence warm deep water transport onto the Amundsen continental shelf, and to what extent its pinning islands loosen (strengthen) their grips on a thinner (thicker) ice shelf.

[22] **Acknowledgments.** We thank the many individuals who have assisted with data acquisition and processing, R. Guerrero, D. Shoosmith, and S. Stammerjohn for CTD observations from other ships and *NB Palmer* cruises, and reviewers for constructive comments. This work was supported by NSF grants ANT-0632282, ANT-0440775, and OPP-9725024, and NOAA award NA08OAR4320912 to Columbia University, NERC grant NE/G001367/1 to the British Antarctic Survey, NASA grants NNX08AN28A and NNX10AV16G to the University of California, Irvine, and by the Lamont-Doherty Earth Observatory, contribution 7717.

## References

Alberts, F. G. (1995), *Geographic Names of the Antarctic*, 2nd ed., NSF 95-157, pp. 834. [Available at <http://archive.org/details/GeographicNamesOfTheAntarctic2ndEdition>.]

Arneborg, L., A. K. Wahlin, G. Bjork, B. Liljebladh, and A. H. Orsi (2012), Persistent inflow of warm water onto the central Amundsen shelf, *Nat. Geosci.*, *5*, 876–880, doi:10.1038/NCEO1644.

Assmann, K. M., and R. Timmermann (2005a), Variability of dense water formation in the Ross Sea, *Ocean Dyn.*, *55*, 68–87, doi:10.1007/s10236-004-0106-7.

Assmann, K. M., H. H. Hellmer, and S. S. Jacobs (2005b), Amundsen Sea ice production and transport, *J. Geophys. Res.*, *110*, C12013, doi:10.1029/2004JC002797.

Comiso, J. C., R. Kwok, S. Martin, and A. L. Gordon (2011), Variability and trends in sea ice extent and ice production in the Ross Sea, *J. Geophys. Res.*, *116*, C04021, doi:10.1029/2010JC006391.

Dinniman, M. S., J. M. Klinck, and E. E. Hofmann (2012), Sensitivity of circumpolar deep water transport and ice shelf basal melt along the west Antarctic Peninsula to changes in the winds, *J. Clim.*, *25*, 4799–4816, doi:10.1175/JCLI-D-11-00307.1.

Fretwell, P., et al. (2013), Bedmap2: Improved ice bed, surface and thickness data sets for Antarctica, *Cryosphere*, *7*, 375–393, doi:10.5194/tc-7-375-2013.

Hall, A., and M. Visbeck (2002), Synchronous variability in the southern hemisphere atmosphere, sea ice, and ocean resulting from the annular mode, *J. Clim.*, *15*, 3043–3057.

Hellmer, H. H. (2004), Impact of Antarctic ice shelf basal melting on sea ice and deep ocean properties, *Geophys. Res. Lett.*, *31*, L10307, doi:10.1029/2004GL019506.

Holland, P. R., and R. Kwok (2012), Wind-driven trends in Antarctic sea-ice drift, *Nat. Geosci.*, *5*, 872–875, doi:10.1038/NCEO1627.

Holland, P. R., A. Jenkins, and D. M. Holland (2010), Ice and ocean processes in the Bellingshausen Sea, Antarctica, *J. Geophys. Res.*, *115*, C05020, doi:10.1029/2008JC005219.

Jacobs, S. S., and C. F. Giulivi (2010), Large multidecadal salinity trends near the Pacific-Antarctic continental margin, *J. Clim.*, *23*, 4508–4524, doi:10.1175/2010JCLI3284.1.

Jacobs, S. S., H. E. Huppert, G. Holdsworth, and D. J. Drewry (1981), Thermohaline steps induced by melting of the Erebus Glacier Tongue, *J. Geophys. Res.*, *86*(C7), 6547–6555.

Jacobs, S. S., H. H. Hellmer, and A. Jenkins (1996), Antarctic ice sheet melting in the southeast Pacific, *Geophys. Res. Lett.*, *23*(9), 957–960, doi:10.1029/96GL00723.

Jacobs, S. S., P. A. Mele, G. Krahnmann, and W. M. Smethie (2002), Coastal Ocean Measurements in the Amundsen and Ross Seas, *NB Palmer Cruise 00-01, Tech. Rep. LDEO-2002-2a*, pp. 366, Lamont-Doherty Earth Observ., Palisades, N. Y., Feb–Mar.

Jacobs, S. S., A. Jenkins, C. F. Giulivi, and P. Dutrieux (2011), Stronger ocean circulation and increased melting under Pine Island Glacier ice shelf, *Nat. Geosci.*, *4*, 519–523, doi:10.1038/ngeo1188.

Jacobs, S., A. Jenkins, H. Hellmer, C. Giulivi, F. Nitsche, B. Huber, and R. Guerrero (2012), The Amundsen Sea and the Antarctic ice sheet, *Oceanography*, *25*(3), 154–163.

Jenkins, A. (1999), The impact of melting ice on ocean waters, *J. Phys. Oceanogr.*, *29*, 2370–2381.

Jenkins, A., and S. S. Jacobs (2008), Circulation and melting beneath George VI ice shelf, Antarctica, *J. Geophys. Res.*, *113*, C04013, doi:10.1029/2007JC004449.

Jenkins, A., P. Dutrieux, S. S. Jacobs, S. D. McPhail, J. R. Perrett, A. T. Webb, and D. White (2010), Observations beneath Pine Island Glacier in West Antarctica and implications for its retreat, *Nat. Geosci.*, *3*, 468–472, doi:10.1038/ngeo890.

Klinck, J. M., and M. S. Dinniman (2010), Exchange across the shelf break at high southern latitudes, *Ocean Sci.*, *6*, 513–524, doi:10.5194/os-6-513-2010.

Lenaerts, J. T. M., M. R. van den Broeke, S. J. Dery, E. van Meijgaard, W. van de Berg, S. P. Palm, and J. S. Rodrigo (2012), Modeling drifting snow in Antarctica with a regional climate model: 1. Methods and model evaluation, *J. Geophys. Res.*, *117*, D04108, doi:10.1029/2011JD016145.

Martinson, D. G., and D. C. McKee (2012), Transport of warm upper circumpolar deep water onto the western Antarctic Peninsula continental shelf, *Ocean Sci.*, *8*, 433–442, doi:10.5194/os-8-433-2012.

Nitsche, F. O., S. S. Jacobs, R. Larer, and K. Gohl (2007), Bathymetry of the Amundsen Sea continental shelf: Implications for geology, oceanography and glaciology, *Geochem. Geophys. Geosyst.*, *8*, Q100009, doi:10.1029/2007GC001694.

Olbers, D., and H. Hellmer (2010), A box model of circulation and melting in ice shelf caverns, *Ocean Dyn.*, *60*, 141–143, doi:10.1007/s10236-009-0252-z.

Padman, L., et al., (2012), Oceanic controls on the mass balance of Wilkins ice shelf, Antarctica, *J. Geophys. Res.*, *117*, C01010, doi:10.1029/2011JC007301.

Phillips, O. M. (1970), On flows induced by diffusion in a stably stratified fluid, *Deep Sea Res.*, *17*(3), 435–443.

Pritchard, H. D., R. J. Arthern, D. G. Vaughan, and L. A. Edwards (2009), Extensive dynamic thinning on the margins of the Greenland and Antarctic ice sheets, *Nature*, *461*, 971–975, doi:10.1038/nature08471.

Pritchard, H. D., S. R. M. Ligtenberg, H. A. Fricker, D. G. Vaughan, M. R. van den Broeke, and L. Padman (2012), Antarctic ice-sheet loss driven by basal melting of ice shelves, *Nature*, *484*, 502–505, doi:10.1038/nature10968.

Rignot, E. (2008), Changes in West Antarctic ice stream dynamics observed with ALOS PALSAR data, *Geophys. Res. Lett.*, *35*, L12505, doi:10.1029/2008GL033365.

Rignot, E., J. L. Bamber, M. R. Van den Broeke, C. Davis, Y. Li, W. J. Van de Berg, and E. Van Meijgaard (2008), Recent Antarctic ice mass loss from radar interferometry and regional climate modeling, *Nat. Geosci.*, *1*, 106–110, doi:10.1038/ngeo102.

Rignot, E., J. Mouginot, and B. Scheuchl (2011a), Antarctic grounding line mapping from differential satellite radar interferometry, *Geophys. Res. Lett.*, *38*, L10504, doi:10.1029/2011GL047109.

Rignot, E., J. Mouginot, and B. Scheuchl (2011b), Ice flow of the Antarctic ice sheet, *Science*, *333*(6048), 1427–1430.

Rignot, E., S. Jacobs, J. Mouginot, and B. Scheuchl (2013), Ice shelf melting around Antarctica, *Science*, *341*(6143), 266–270.

Robertson, R. (2013), Tidally induced increases in melting of Amundsen Sea ice shelves, *J. Geophys. Res.*, *118*, 3138–3145, doi:10.1002/jgrc.20236.

Schodlok, M. P., D. Menemenlis, E. Rignot, and M. Studinger (2012), Sensitivity of the ice shelf ocean system to the sub-ice shelf cavity shape measured by NASA IceBridge in Pine Island Glacier, West Antarctica, *Ann. Glaciol.*, *53*(60), 156–162, doi:10.3189/2012AOG60A073.

Schoof, C. (2010), Beneath a floating ice shelf, *Nat. Geosci.*, *3*, 450–451.

Shepherd, A., D. Wingham, and E. Rignot (2004), Warm ocean is eroding West Antarctic ice sheet, *Geophys. Res. Lett.*, *31*, L23402, doi:10.1029/2004GL021106.

Shepherd, A., D. Wingham, D. Wallis, K. Giles, S. Laxon, and A. V. Sundal (2010), Recent loss of floating ice and the consequent sea level contribution, *Geophys. Res. Lett.*, *37*, L13503, doi:10.1029/2010GL042496.

Simmons, A., S. Uppala, D. Dee, and S. Kobayashi (2006), ERA-Interim: New ECMWF reanalysis products from 1989 onward, *ECMWF Newsletter*, *110*, 25–35.

St-Laurent, P., J. M. Klinck, and M. S. Dinniman (2013), On the role of coastal troughs in the circulation of warm circumpolar deep water on Antarctic shelves, *J. Phys. Oceanogr.*, *43*, 51–64, doi:10.1175/JPO-D-0237.1.

- Stammerjohn, S. E., D. G. Martinson, R. C. Smith, X. Yuan, and D. Rind (2008), Trends in Antarctic annual sea ice retreat and advance and their relation to El Niño-Southern Oscillation and Southern Annular Mode variability, *J. Geophys. Res.*, *113*, C03S90, doi:10.1029/2007JC004269.
- Swithinbank, C., R. S. Williams, J. G. Ferrigno, K. M. Foley, and C. E. Rosanova (2003a), *Coastal-Change and Glaciological Map of the Bakutis Coast Area, Antarctica: 1972–2002*, 2nd ed., U.S. Geol. Surv. Geol. Invest. Ser. Map, I-2600-F.
- Swithinbank, C., R. S. Williams, J. G. Ferrigno, K. M. Foley, C. A. Hallam, and C. E. Rosanova (2003b), *Coastal-Change and Glaciological Map of the Saunders Coast area, Antarctica: 1972–1997*, U.S. Geol. Surv. Geol. Invest. Ser. Map, I-2600-G.
- Timmermann, R., Q. Wang, and H. H. Hellmer (2012), Quantification of ice shelf basal melting using a global finite-element sea ice—ice shelf—ocean model, *Ann. Glaciol.*, *53*(60), 303–314, doi:10.3189/2012AoG60A156.
- Wahlin, A. K., X. Yuan, G. Bjork, and C. Nohr (2010), Inflow of warm circumpolar deep water in the central Amundsen shelf, *J. Phys. Oceanogr.*, *40*, 1427–1434, doi:10.1175/2010JPO4431.1.
- Yager, P. L., et al. (2012), The Amundsen Sea polynya international research expedition, *Oceanography*, *25*(3), 40–53.
- Zwally, H. J., and M. B. Giovinetto (2011), Overview and assessment of Antarctic ice-sheet mass balance estimates: 1992–2009, *Surv. Geophys.*, *32*, 351–376, doi:10.1007/s10712-011-9123-5.
- Zwally, J. H., M. B. Giovinetto, J. Li, H. G. Cornejo, M. A. Beckley, A. C. Brenner, J. L. Saba, and D. Yi (2005), Mass changes of the Greenland and Antarctic ice sheets and shelves and contributions to sea-level rise: 1992–2002, *J. Glaciol.*, *51*(175), 509–527.